# Surface Deformation and Gravity Changes from Surface and Internal Loads

# Final Report

By Bradford H. Hager and Ming Fang

Table of Contents

# 1. UPDATED OBJECTIVES

## 1.1 The new challenges

Aero and space borne remote sensing have made it possible to monitor the mass and energy transport at various scales within the cryosphere-hydrosphere-atmosphere system. The recent surface mass balance (the rate of net gain of snow and ice at a geographic point) map for the Antarctic ice sheet is constructed by interpolating sparse in situ observations (about 1,800 points) with empirically calibrated satellite data of passive back emission of microwaves (Vaughan et al, 1999). The digital elevation model obtained from satellite radar altimetry is used to improve the delineation of the ice flow drainage basins (Bamber, 1994; Bamber and Huybrechts, 1996; Vaughan et al, 1999). As important as these results are, the uncertainty remains up to about ±2mm/yr. of eustatic sea level change with the net imbalance (Jacobs et al, 1992; Vaughan et al, 1999). In other words, we are still unable to determine even the sign of the contribution of the Antarctic ice sheet to contemporary sea level change. The problem is more likely with the discharge rather than accumulation.

Transition from snowfalls to an icy layer can be regarded as a process of gravitational stabilization, a process may take centuries (e.g. Liboutry, 1998). Therefore, the in situ observations in the accumulation zones, i.e. most of the surface cover of Antarctic, can be progressively updated and back checked to further constrain the accuracy of mass balance maps (Bull, 1971; Giovinetto and Bentley, 1985; Vaughan et al, 1999). The opposite is true for the processes of attrition and ablation. The surge and collapse of ice streams are nonlinear functions of a number of dynamic variables and empirical parameters, few of which are well constrained. Satellite radar altimetry with the footprint of tens of kilometers is not adequate for monitoring the surge and collapse of ice streams. The technique of interferometry could recover the discharge of streams from the elevations observed with synthetic aperture radars (Rignot et al, 1996; Rignot, 1997; 1998), yet the irregular topographies, including the calving ice walls and melting ice lobes at the ice sheet margin, often corrupt the fringes. The highest resolution is achieved by laser altimetry with footprints of only tens of meters. Even with perfect altimetry, uncertainty in the inference of mass balances is still not well constrained without addressing the issues of unstable snow masks, unknown local density profiles, unknown internal flows, crustal responses etc.

Basal lubrication and friction (often due to the roughness of the ice-bed interfaces) have strong control over the sliding and viscous deformation of the lower part of the ice stream. Thus, on the verge of break up, when shear stresses are released, the change in surface elevation may not synchronize with the flow in the lower part of the ice sheets. Crustal deformation in response to the ice mass redistribution, known as glacial isostasy, is not only an error source for the inference of mass balance with altimetry, it feeds back to the control mechanism for the advance or retreat of ice sheets (Hughes, 1987; Denton et al, 1992; Hughes, 1998). As is well known, the residual crust uplift since the termination of the last Quaternary cycle is a source of error for using altimetry to infer the change of ice sheet thickness in the Greenland and Antarctic areas. At the same time, it is

a major source of data for the study of mantle rheology (e.g.Peltier & Andrews 1976; Mitrovica & Peltier, 1993, Hager, 1989; Fang & Hager, 1996, 1999).

A cross constraint for the ice mass imbalances is the sea level change. The 1-2 mm/yr sea level increase derived from tidal gauge records (Douglas, 1991, 1997; Woodworth et al, 1992) has been of great interest in recent years for its close relation to the publicized issue of global warming. But the physical significance of these figures is limited by the terribly sparse and uneven distribution of tidal gauge records. Even a static ocean cannot be perturbed uniformly (Farrell & Clark, 1976; Dahlen, 1976; Conrad & Hager, 1997; Fang & Hager, 1999; Mitrovica et al. 2001). Most of the published results are based on tidal observations along the North Atlantic coasts. It is unclear if these measured sea level rises apply to other coastal areas all over the world, and more uncertain of how it represents the entire sea level change associated with the ice mass imbalance, because static changes in the magnitude of 1-2mm/yr can be easily over shadowed by low frequency ocean circulation modes (Wunsch, personal communication).

### 1.2 Adjusted research strategy

In response to the new challenges, we adjusted our main goal of this project to establishing new constraints for the mass balances, and more importantly the total imbalances, in the Greenland and Antarctic areas by quantifying their signatures from gravity observations of different scales, local regional, and global.

*For local analysis*, it was first suggested by our group to utilize the observed crustal deformation to "weigh" the time variation of ice sheets (Hager, 1991). This idea was modified and tested by Wahr's group (Wahr et al, 1995; Wahr & Han, 1998; Larson & van Dam, 2000). The basic technique in Wahr's method is to combine the GPS vertical and absolute gravity measured at the same sites near the margin of ice sheets to remove the ancient signals from postglacial rebound to avoid it being mistaken as due to modern glacial change. There are two issues left by their analysis: (i) independence of the technique on the largely unconstrained mantle viscosity structures, (ii) the formulation for quantifying the ice signature in the combined observables. We solved the first problem during this project and published the results (Fang & Hager, 2001). Details of the results and current progress will be outlined in section 2.

*For regional analysis*, we developed and implemented the technique of spherical wavelets. A wavelet transform is to use a small wave of zero mean, scaled and translated, to scan through the space of data.

A unique quality of wavelets is its ability to isolate and enhance small, however small, and discontinuous features, thus, it is ideal for localized data sets with irregular boundaries and sharp contrasts such as the distribution of ice sheets, plume like structures in seismic tomography (e.g. Bethoux et al, 1998; Bergeron et al. 1999; Bergeron et al, 2000). Another noticeable quality of wavelets is that it provides spatial and harmonic (frequency) localization simultaneously (subject to Heisenberg's uncertainty principle). This is especially important for gravity analysis, which is a highly lumped signal.

We worked on spherical wavelets in 1994 in collaboration with Dr. Mark Simons, then at MIT. We independently constructed what is equivalent to the locally supported spherical wavelet of Freenen & Windhuser (1996) employed in tracing the source of the conspicuous gravity low in the Hudson Bay area (Simons & Hager, 1997). The general

theory for spherical wavelets has been developed by Freenen & Windhuser (1996, 1997). Since we all use small waves (non-uniform windows) as a set of spherical caps with wiggled cross sections, we shall call them isotropic spherical wavelets (ISW). We applied wavelets to characterize the Last Quaternary ice sheets, and to quantify the exponential-like relaxation curves near the centers of the ice sheets. Results of these works are published (Fang & Hager, 2002). Our current investigation is on quantifying the mass balance signatures of the Greenland and Antarctic Ice sheets. The published results and ongoing progress will be outlined in section 3.

*For global analysis*, we look at the lower degree harmonic coefficients (e.g. Cheng et al, 1997). These low degree coefficients are powerful constraints for the total mass redistribution. Yet they are highly lumped signals, even the core may have a contribution (Fang et al, 1996). We have found during this NASA investigation that the time varying harmonic coefficients, as low as degree3, are sensitive to the ice history. There have been a number of follow up confirmations, since we first reported the result to an IAG assembly in 2000. Currently, we are collaborating with the group of the Center of Space research at Texas University to further quantify the sensitivity. This part of the work is reported in section 4.

*For sea level analysis*, In conjunction with previous NASA project, we have succeeded, during this investigation, in formulating and implementing the equilibrium sea level by means of least potential energy principle (Fang & Hager, 1999). The theory could be extended to a non-equilibrium ocean by including the non-gravitational forces and local tectonics to address the issue of mass budget in the ocean. But the latter idea is a little too ambitious. Collaborative efforts are being made by our group and the geodetic group in the Hong Kong Polytech. University on the analysis of tidal gauge records; details will be reported in section 5.

## 2. PROGRESS OF LOCAL ANALYSIS

### 2.1 Published results

An increasing number of instruments, including superconducting gravimeters, absolute gravimeters, and GPS receivers have been operating in the Greenland and Antarctic regions. Crustal deformation in these areas is strongly influenced by both postglacial rebound and contemporary ice mass redistribution. To quantify the ice mass signature, we first have to get rid of the ancient signals. We seek to determine whether, when the viscosity profile in the Earth's interior is unknown, the effects of viscous relaxation in the memory of surface mass change can be separated from the effects of present day mass variation by combined measurements of vertical displacement and absolute gravity. The key issue is to establish a relationship between the vertical load Love number $h_n$ and the gravity load Love number $k_n$ at each harmonic degree $n$. We find through dynamic analysis (see Fang & Hager, 2001a for detail) that for an incompressible Earth,

$$k_n(t) = \frac{3}{2}\frac{\tilde{\rho}_n}{(n+1/2)} h_n(t) \quad (n \geq 2) \tag{1}$$

where $\rho_E$ is the average density of the whole Earth, and $\tilde{\rho}_n$ is what we call the pseudo-surface density as a function of harmonic degree *n*.

$$\tilde{\rho}_n = \rho(a) - \int_0 \frac{d\rho(r)}{dr}\left(\frac{r}{a}\right)^{2n+1} dr = \frac{2n+1}{a}\int_0 \rho(r)\left(\frac{r}{a}\right)^{2n} dr \tag{2}$$

The radial integration is from the center of the Earth to the surface *a*.

Equation (1) is independent of rheology parameters in the interior. For PREM model (Dziwonski & Anderson, 1981) the average pseudo-surface density is $<\tilde{\rho}>\approx 3.5$. From (1) and (2) we come up with the analytical expression for the constant *A* deduced empirically by Wahr et al (1995):

$$A = \frac{2a\rho_E}{3g\langle\tilde{\rho}\rangle} \approx 6.5\,\mathrm{mm}/\mu\mathrm{gal} \tag{3}$$

Let us combine the observed vertical deformation *u(t)* with the incremental gravity $\delta g(t)$ by forming the new observable

$$\Delta(t) = u(t) - A\delta g(t) \tag{4}$$

It can be shown that $\Delta$(t) is primarily due to the variation of ice mass (Wahr et al. 1995; Fang & Hager, 2001a). Relation (4) is one of the major steps in local analysis.

For a compressible Earth, equation (10 should be modified as (Fang & Hager, 2001a)

$$k_n(t) = \frac{3}{2}\frac{\tilde{\rho}_n}{(n+1/2)\rho_E} h_n(t) - x_n^e(t) - x_n^v(t) \tag{5}$$

where

$$x_n^\beta = \frac{3}{(2n+1)\rho_E}\int_0 \rho(r) X_n^\beta(r,t)\left(\frac{r}{a}\right)^{n+2} dr \qquad (\beta = e,v) \tag{6}$$

represent the elastic and viscous compressions respectively. We assert that the term of viscous compressibility $x_n^\beta$ is negligible for a Maxwell Earth, since it is viscously incompressible. This assertion is confirmed numerically as shown in Fig. 1, 2 where we generated three markedly different viscosity models (Fig. 1), and then calculate the pseudo-surface densities for each one of the models (Fig. 2). Our assertion is confirmed

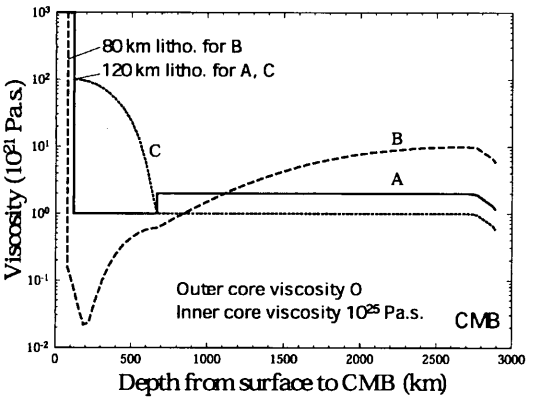


**Fig. 1** Test viscosity models. Model A (solid line) is a fairly uniform profiled advocated by Tushingham & Peltier (1991). We adopt it here as a reference for the two extremes B and C. The lithosphere for model C (short dashed line) is the same as for model A. Model C and B are generated using the empirical parameterization introduced in Fang and Hager (1999).

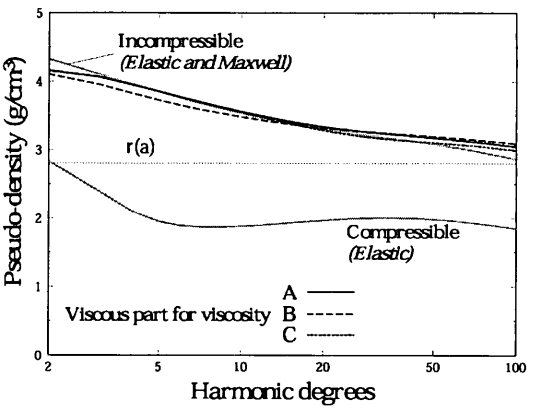


**Fig. 2** Pseudo-surface densities for incompressible and compressible Earth models. The compressible and incompressible elastic $\tilde{\rho}_n$ are displayed with gray lines. The thin dot line indicates the true surface density of the 1066B Earth model. The dark solid, long dashed and short dashed lines are the viscous compressible $\tilde{\rho}_n$ calculated by means of a least square procedure with respect to the time variable.

by the convergence of the viscous pseudo-surface densities of those viscosity models (see details in Fang & Hager, 2001a). We plot in Fig. 3 the predicted present day change of gravity due to postglacial rebound in the Antarctic area for each viscosity model in Fig. 1 along with their residuals. The present rate of residual is defined as $d\delta g/dt = A^{-1}du/dt$ We can see clearly from Fig. 3 that the residuals are about 5% and less in areas where the ice signals are strong. A better reduction of the residuals can be achieved if we replace the average pseudo-surface density with the true pseudo-surface density for each single harmonic. But this procedure is practically meaningless, since it is very difficult to obtain the global harmonic coefficients for the present day vertical deformation field for the crust.

## 2.2 Results to be published

There three issues remain to be solved before we can quantify the ice mass signature from the hybrid observable Δ(t). First, the residual control. The pseudo-surface densities are function of harmonic degrees as we can see from Fig. 2. It is readily shown by examining single harmonic degrees that for the long waveband (degree 2-9), the dominate waveband (degree 10-35), and the short waveband (degree >30), the average values for the constant $A$ are 5.7, 6.4, 7.4 respectively. By taking the procedure (4) and using the constant given by (3), we could characterize the residuals of viscous effect by three residual values of $A$: -0.7, 0.1, and 0.1, respectively representing the three

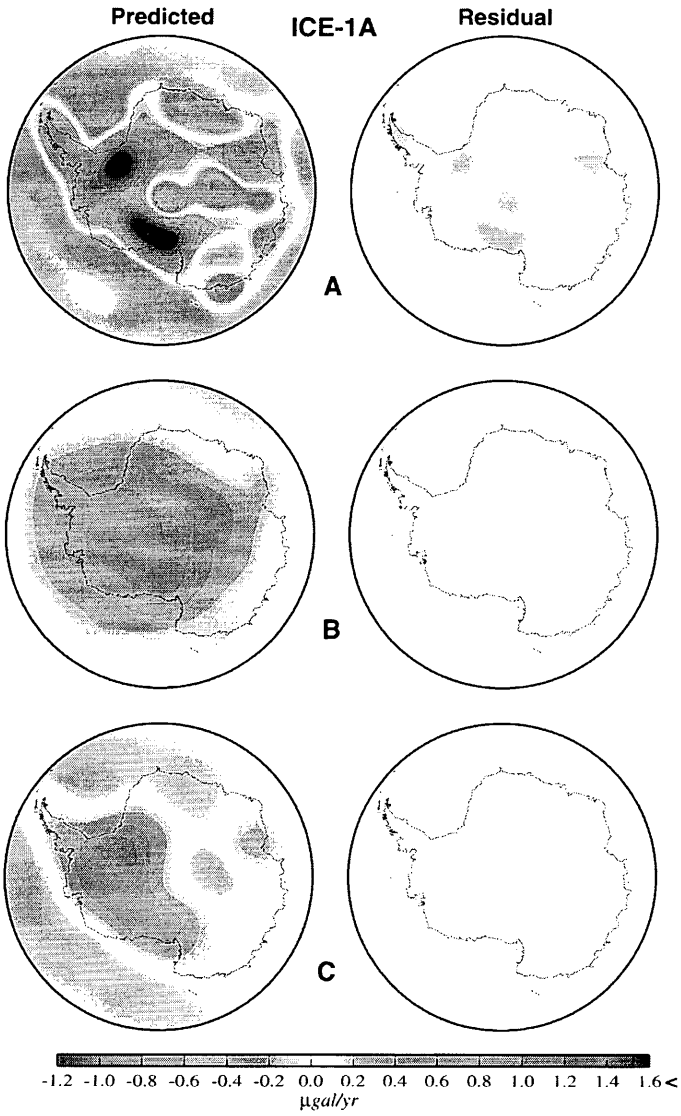


**Fig. 3** Predicted present day rate of change of the gravity field due to postglacial rebound in the Antarctic area and the residuals. Calculation are based on the admissible viscosity models displayed in Fig. 1, and the ice sheet model ICE-1A which is a modified version of the ice model of Peltier & Andrews (1976). Major difference between ICE-1 and ICE-1A happens to occur in the Antarctic area, since ICE-1 is reconstructed on for the northern hemisphere. Antarctic ice is first added by Nakada & Lambeck (1987) based on the Quaternary ice sheet map of Denten & Hughes (1986).

waveband. It is not clear yet whether the simple average (3) is the optimal value for keeping the residuals of the ancient signals minimum. We plan to look at the issue by weighing contributions from the three wavebands. Viscosity is no longer the issue in this task, but ice model is. We are conducting numerical tests on all existing last Quaternary ice sheets models (ICE-1A, ICE-3G, ICE-4G etc) to learn the sensitivity of the optimal solution for $A$ on the ice sheet model. We also plan to scale the Antarctic portion of these ice models artificially to see under what condition the residuals will be out of control. These experiments on Holocene ice models are complimentary to the viscosity control analysis outlined above. We expect to come up with a optimal value of the constant $A$ with an upper bound for its applicability.

The second issue concerns the compression term. Equations (1) to (6) not only represent the physics for removing the postglacial rebound signature, but also the foundation for deconvolutions for modern ice mass signatures (see Fang & Hager, 2001

for details). Effects from elastic compressibility have been perceived in geodetic investigations for Quaternary ice sheets but without formulation (Ekman, 1992; Ekman, & Makinen, 1996). The compression term $x_n^e$ expressed by (6) can be regarded as the compression load Love numbers. They convolute with the ice height variation $\xi$ to give rise to the compressibility correction for gravity disturbance

$$\delta g_x(\theta,\varphi,t) = \frac{ga^2}{M_E}\int \xi(\theta',\varphi',t)\sum_n (n+1)x_n^e \mathrm{P_n}(\cos\alpha)d\Omega' \qquad (7)$$

where $\mathrm{P_n}$ is the Legendre polynomial, $\alpha$ denotes the angle between the fixed point ($\theta$, $\varphi$) and the moving point ($\theta'$, $\varphi'$), $d\Omega$ stands for the area element on the surface of a unit sphere. We are investigating these compression Love numbers on general terms. Note, the familiar gravity kernel $(1+k_n)$ has to be replaced by the new kernel $(1-x_n^e)$ after the removal of postglacial effects. We are conducting systematic forward modeling for the gravity field with both kernels. As an input of the ice mass model, we will adopt the existing mass balance maps for Greenland and Antarctic areas (e. g. Reeh et al. 1999; Zwally & Giovinetto (2000); Vaughan et al. 1999). Special attention is paid to the short waveband. The short waveband is not affected significantly by postglacial rebound, but it may have significant effects from modern ice mass balance, especially in the areas of ice sheet margins where most of the polar stations are located.

The third issue that we are dealing with is about the distribution of sites. Application of our formulation to analyze the data collected from the polar stations is straightforward. Three or four sites can only serve as benchmarks for constraining the regional mapping of mass balances, although they are extremely important benchmarks. Taking advantage of the knowledge learned from the work outlined above, we are investigating the possible distribution with minimum number of gravity-GPS stations for a robust constraint of the ice mass redistribution. As far as we know, several projects are already underway for similar goals. What makes our method unique is that with solid physics and explicit formulations (1) to (6) (also see Fang & Hager, 2001 for more) we could go beyond pure empirical experiments in dealing with the separation of ancient secular ice signatures and modern short period ice signatures, and in quantifying the ice mass balances in the combined observables. An important application of the technique of combination is to combine the laser altimetry with the time varying gravity like the GRACE data (this is already beyond local analysis) for the estimate of ice mass balance. The basic idea of such combination was suggested by Wahr & Han, (1998) and tested empirically by Velicogna & Wahr (2000). It is relatively easy for GRACE to separate the secular term (presumably the postglacial rebound signal) and short period terms (here we ignore the uncertainties associated with the unknown continental hydrological system and inadequate lifespan just for the sake of discussion). It is not easy however to isolate the secular terms from altimetry observations, since altimetry only measures the ice surface rather than the basal surface. We propose to calibrate the secular term isolated from the GRACE gravity rates to derive the postglacial rebound correction for altimetry, by using the basic formulation (1), (2), (5), and (6). Here we skip Wahr's relations (4), because GRACE and altimetry data could come in harmonic degrees, therefore, we could perform

the combinations degree by degree using the exact relation (1)! This has not been tested before. We believe that it will yield exciting results in terms of removing the post glacial rebound effect from the laser altimetry, thus, give rise to a robust constraint on the mass balances in Greenland and Antarctic areas. The combination technique could even extended to spherical wavelet analysis which we will elaborate in the next section.

## 3. PROGRESS OF REGIONAL ANALYSIS

### 3.1 Published results

Ice mass in Greenland and Antarctic areas are confined to their continent beds by surrounding oceans. This is the main reason, aside from its unique qualities, we employ spherical wavelets for regional analysis. Here we demonstrate how wavelets is used to characterize the Laurentide and Fannoscandian Holocene ice sheets and to constrain the mantle viscosity structure. These are the long wavelength problems as oppose to the short wavelength contemporary ice mass balance problems. But the basic technique is shared by both problems. Since the technique is not popular yet, we include some background in the problem description.

A unique feature shared by the two major Holocene ice sheets, Laurentide and Fennoscandia is the apparent exponential RSL curves at their central regions. This unique feature laid the foundation for Haskell's (1935) classic analysis to derive the relaxation time $\tau$ for a single exponential mode $\exp(-t/\tau)$, at the characteristic wavelength of the Fennoscandia ice load. In order to achieve an exact exponential mode in a half space, the real ice dome has to be distorted into an exact harmonic undulation extending to infinity. An opposite approach to recover the apparent exponential RSL is to preserve the physical integrity of the ice dome by summing up all harmonics. The later approach has become standard in modern studies (e.g., Farrell & Clark, 1976; Peltier, 1976; Lambeck et al. 1990; Mitrovica, 1996; Fang & Hager, 1999). The so called decay time $T$ in Mitrovica's (1996) analysis is identical with Haskell's relaxation time in the sense that they are obtained from fitting the same curves by essentially identical expressions (different only in spatial and temporal references). But there is a fundamental difference: a decay time is obtained by fitting a RSL curve calculated by summing up all harmonic degrees.

The question here is whether the distribution and the history of retreat of an ice sheet can make the ice-ocean-earth system to achieve a state where the exponential like RSL at its center is related to a single harmonic relaxation without sacrificing the physical integrity of the ice dome. This is analogous to the problem Heisenberg encountered, which leads to his famous uncertainty principle. According to the uncertainty principle, the answer is no, because Haskell's problem is to seek an exact harmonic localization and the modern approach (e.g., Mitrovica, 1996) is to seek an exact spatial localization. It is impossible to achieve both simultaneously. On the other hand, also according to the uncertainty principle, a compromise state could be reached at the expense of ambiguities in both spatial and harmonic localization. The robustness of a spatial or a harmonic localization depends on the physics of the system. We use ISW to quantify such a state, and dynamic analysis to test the robustness of harmonic localization.

The most appealing feature of a locally supported ISW for our purposes is its close relation to a smooth window. The bandpass filter is nearly symmetric about the central frequency (see Fig. 5 below). Mathematically, a spatial localization by an window in the spatial domain corresponds to a harmonic localization in the form of a band-pass filter in the harmonic domain. The size of the window and the width of the filter are related by the famous "uncertainty principle" first quantified by Heisenberg in his dealings with the wave-particle duality of electrons.

To demonstrate the effectiveness of ISW, we plot in Fig. 4 (left) the ISW transform along the 60° latitude profile, called a spectrogram, for the satellite gravity disturbance (Nerem et al, 1994). We choose this small circle because it is approximately the latitude for both centers of Laurentide and Fenoscandia ice sheets. Thus, we can localize both major ice sheets simultaneously. As we can see from Fig. 4 (left) none of the small scale features in the gravity profile along the 60° latitude are lost in the spectrogram. The half angle of support in degree annotated on the left of the spectrogram characterizes the size or scale of the windows, the center wave number on the right indicates the central harmonic of the band-pass filter representing its bandwidth of a particular window. In other words, the spectrogram simultaneously reveals the spatial and harmonic localizations. Two major gravity lows are easily identified in Fig 4 (left): West Siberian Plain and Hudson Bay. The spectrogram in the West Siberian Plain area is rather dispersed; in contrast, the gravity low in the Hudson Bay area is heavily localized at harmonic degree 9, remarkably similar to the surface distribution of currently available models of the Laurentide ice sheet. This is one of the major arguments that led Simons & Hager (1997) to conclude that the gravity low in the Hudson Bay area does have a close association with incomplete rebound following the deglaciation.

Since there is no direct observation of the history of the geoid off the shorelines, the only way we can reconstruct the RSL on the entire surface is through modeling. We adopt ice model ICE-1A as described above.

Assuming the Earth is laterally homogeneous self-gravitating viscoelastic Maxwell body with its elastic parameters controlled by seismic inversion (Dziewonski & Anderson, 1981), the unknown radial viscosity profile is a major uncertainty if we want calculate the RSL at specified sites. But if our goal is to extract the long wavelength global pattern of geoid perturbation induced by deglaciation, the viscosity profile is much less a problem. In fact, we tried a number of viscosity models generated by our recently designed parameterization (Fang & Hager, 1999), and always come up with similar spectrogram as shown in Fig. 4 (right) where we deliberately leave the viscosity unspecified. The physics behind this observation is simple: the response of the solid Earth is laterally homogeneous if the rheology is laterally homogeneous. Thus, the heterogeneity of the geoid is mainly controlled by the irregular distribution of the ice sheets over the surface. Differences in viscous relaxation times resulting from differences in radial viscosity profiles only determines how fast detailed information of ice sheets is lost rather than altering the pattern revealed by the spectrogram. The ISW spectrogram of the predicted RSL in Fig. 4(right) is calculated at 9 kyr before present time (B.P.) A major portion of the ice sheets at this particular time has already melted. What is revealed in Fig. 4 (right) is primarily the viscoelastic relaxation of the solid Earth. We can clearly see the harmonic localization at about degree 9 in the central

region of the Laurentide ice, which is consistent with the previous result of Simons & Hager (1997), while the harmonic localization of the central region of the Fennoscandia ice sheet is at degree 16. The bandpass filters at the two specific centers are displayed in Fig. 5. The difference in harmonic localization is due to the fact that the Laurentide ice sheet covers a broader area than the Fennoscandian. Rebound signals at the center of an ice sheet reflect an average effect of the entire ice load. A broader spatial coverage is equivalent to a poorer spatial localization, which will result in a sharper harmonic localization, as controlled by the uncertainty principle.

The significant bandwidth in the harmonic domain (Fig. 2) raises doubt whether the harmonic localizations revealed from the ISW spectrogram truly mean a single harmonic

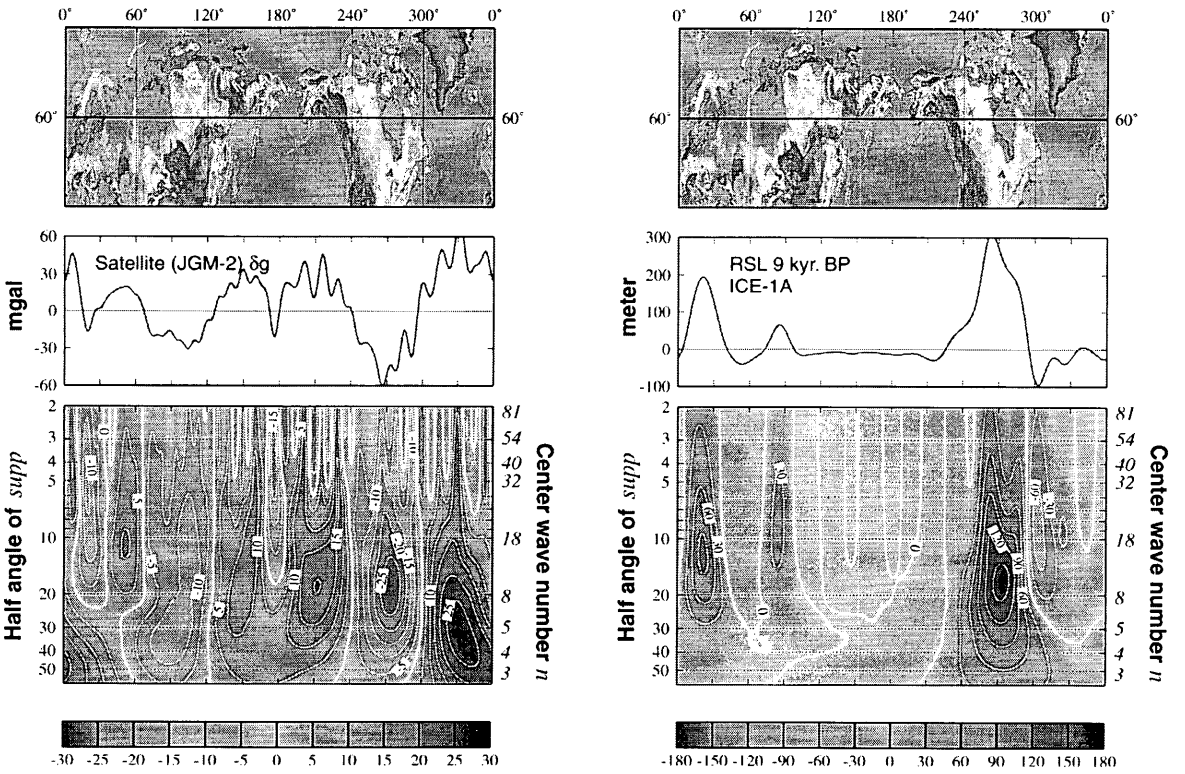


**Fig. 4** (Left) observed satellite gravity disturbance along the 60 degree latitude and the wavelet spectrogram of the gravity disturbance. The translation operation of the wavelets are centered along the 60 degree latitude. Half angles of support (scaled windows) are annotated on the left, representing the spatial localization. The corresponding central harmonics are annotated on the right, representing the harmonic localization. The contour values are set for reference of sensitivity, they are not scaled to any physical unit. (Right) Predicted relative sea level (RSL) 9 kyr before present time along the 60 degree latitude and the wavelet spectrogram of the RSL. Since the static sea level coincides with the geoid, we extend the meaning of sea level to the land as the geoid variation, thus, the IWS transform can be performed all over the globe. The calculation is based on the modified ice model, ICE-1A. We do not specify the viscosity here because for a laterally homogeneous model, the pattern of the wavelet spectrogram is insensitive to the viscosity profile.

dominant in the observed exponential like curves at the centers of the ice sheets. We look into this issue by comparing the decay time diagram of Mitrovica (1996) with the relaxation time diagram for single harmonics (Fig. 6). Mitrovica and Peltier (1993; 1995) parameterized the RSL curves in the central region of the major ice sheets by a single exponential form

$$H(t) = A\left(\exp(t/T) - 1\right) \tag{8}$$

where $H(t)$ denotes the height of the RSL at a specific site, $A$ and $T$ are the parameters determined by fitting the RSL curve at the site. The time, $t$, here is measured as positive backwards before the present time. Obviously, the RSL $H(t)$ is a lumped signal of all harmonic degrees governed by the sea level equation (Farrell and Clark, 1976). To distinguish between the parameter $T$ and the relaxation time for a single harmonic degree, $\tau$, we follow Mitrovica (1996), calling $T$ a decay time. Assuming a two layer viscosity model with fixed lithosphere and ice model, one can find that the decay time is a function of the upper mantle viscosity $\eta_u$ and the lower mantle viscosity, $\eta_l$

$$T = T(\eta_{um}, \eta_{lm}) \tag{9}$$

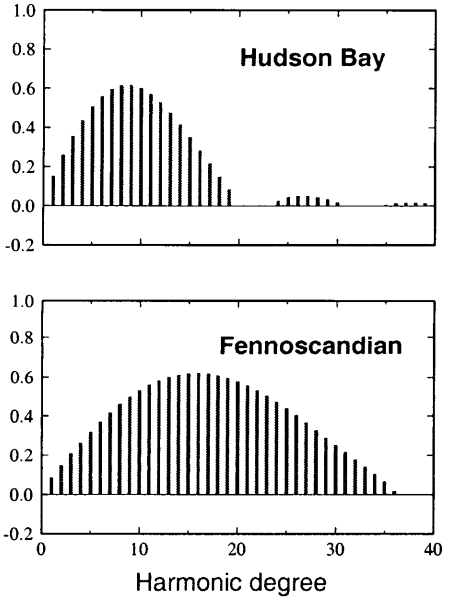


**Fig. 5** Harmonic spectra of the IWS transforms at the centers of the two major ice sheets. Angle of supports (windows) are set about the same sizes of the two ice sheets. They all in the form of bandpass filter as discussed in the text.

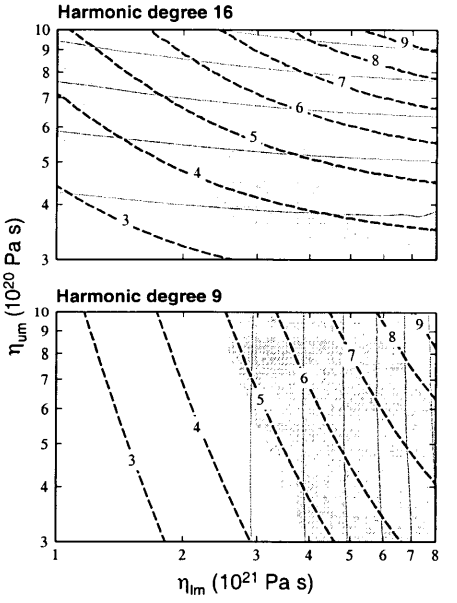


**Fig. 6**. Relaxation diagram s of degree 16 and 9. Shaded areas are adopted from Mitrovica (1996) for comparison. Thin dot lines are the relaxation diagrams for degree 25 (top) and degree 4 (bottom).

For a fixed value of $T$, equation (2) determines an iso-contour in the $\eta_u$~$\eta_l$ plane called the decay time diagram. In creating decay time diagrams, Mitrovica (1996) summed up harmonic degrees up to 256 to calculate the predicted RSL, $H(t)$, at the centers of disk ice loads simulating the Laurentide and Fennoscandia ice sheets. He then fit the observed RSL curves over the last 9 kyr at Angermanland Sweden, the center of the Fennoscandia ice sheet, and over the last 6.5 kyr at Richmond Gulf, Southeastern Hudson Bay, the center of the Laurentide ice sheet.

For comparison, we generate a relaxation time diagram in Fig. 6 following a similar procedure to Mitrovica's (1996) decay time diagram: assuming a two layer viscosity model with a fixed lithosphere

$$\tau = \tau(\eta_{um}, \eta_{lm}) \tag{10}$$

For a constant value of $\tau$, equation (10) determines an iso-contour in the $\eta_u$~$\eta_l$ plane, called a relaxation time diagram.

We pick the degree 16 relaxation diagram to compare with the decay time diagram at Angerman land, and the degree 9 relaxation time diagram to compare with the decay time diagram at Richmond Gulf. Simultaneous matches in slope can be found in both the degree 16 (Angerman land) and degree 9 (Richmond Gulf) cases. Slopes are in fact the most diagnostic factor in identifying the harmonic degree in the relaxation diagram: the transition from lower degrees through intermediate degrees to higher degrees is very regular and can be clearly identified from the slopes of the iso-contours (compare the thin lines with the thick lines in Fig. 3). Thus, this simultaneous match in slopes strongly suggests that the decay times are indeed akin to the relaxation times of single harmonic degrees.

In addition to the good fits in slope, the degree 16 relaxation diagrams (Fig. 6) match especially well with their Angermanland counterparts (Mitrovica's (1996) Fig. 4a) indicating a strong boost of degree 16 as a result of strong cancellations among the flanking degrees in the bandpass filter. As with the degree 9 relaxation diagrams compared to the Richmond Gulf decay diagrams, there are noticeable shifts in the relaxation diagram with reference to the decay diagram. For instance, the 6 kyr contour of the relaxation diagram locates approximately at the place of 6.6 kyr contour of the decay diagram, making about a 10% shift in iso-value. The largest of such shifts is about 20% by the 3 kyr contour. These discrepancies represent relatively larger ambiguity in relating the RSL to a single harmonic, as a result of poorer cancellation among the flanking degrees in the bandpass filter.

Mitrovica and Peltier (1995) have found through numerical tests that if we only consider the time range in which the RSL change is dominated by free rebound, the decay time $T$ is relatively insensitive to the details of the ice history. This observation can be easily explained if we interpret the decay times as strong signature of the relaxation times of single degrees, since the relaxation times are independent of ice models. Conversely, this observation indirectly supports our conclusion that the decay times, subject to ambiguities, represent single harmonic degrees. Our results indicate that the lateral heterogeneity in mantle rheology that affect the post glacial rebound is rather weak.

They also provide a new constraint on the relaxation spectrum first obtained by McConnell (1968) and rederived recently by Wieczerkowski et al. (1999) based on uplifted strandlines in the Fennoscandia area (Fig. 7). As shown in Fig. 7, the relaxation spectrum plays a crucial role in the inference of the mantle viscosity profile, especially in constraining the thickness of the lithosphere and the upper mantle viscosity structure. Detailed discussion on the relaxation spectrum and the viscosity structure is referred to Fang & Hager (2001).

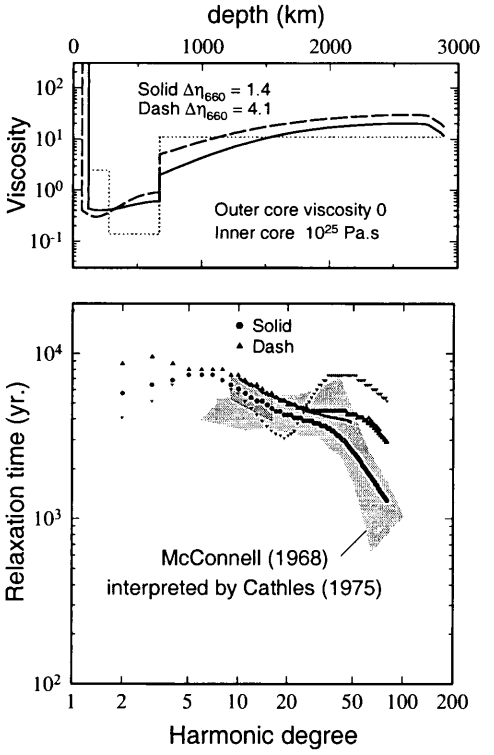


**Fig. 7.** Relaxation spectra and the preferred viscosity models. McConnell's (1968) spectrum with its error bars as interpreted by Cathles (1975) is plotted in the blue area. The yellow parallelogram represents a linear interpolation between degree 9 and degree 16 of our new results from wavelet analysis and the curve fitting based on the observed RSL at the centers of the ice sheets. The red line represents the spectrum from degree 10 to 75 recently rederived by Wieczerkowski et al (1999). Plotted in the background as grey dots and inverse triangles are the viscosity model proposed by Simons and Hager (1997) and the relaxation spectrum associated with it. Viscosity $\eta$ is in the unit of 10**21 Pas.

### 3.2 Results to be published

The largest uncertainty in the GRACE data perhaps is the continental underground hydrological system. Its effect could span the entire normal lifetime (5 years) for the GRACE Mission. But the signatures of the hydrological system could be easily identified by a wavelet analysis, since the distribution of the underground reservoirs must be regionalized or localized within their residing continents. We would like to address the hydrology issue in a separate project. Currently are using a similar principle to quantify the ice mass balances in Greenland and Antarctic areas. We assume in the following discussions that secular terms have been removed from the time varying gravity field derived from GRACE.

Our first objective is to identify the spatial and harmonic localization of the time varying gravity over Greenland and Antarctic. Note, spherical wavelets is a technique of 2D to 4D mapping. The extra 2D space introduces redundancy for reconstruction. The redundancy could be overcome by what is called multi-resolution analysis (see below).

On the other hand, the extra 2D space provides room for zooming into small features and sharp edges like the ice sheet margin. A careful design of the scan contours could yield much more useful information. This idea of contour manipulation is already applied in choosing the 60° degree latitude small circle for characterizing the Laurentide and Fannoscandian Holocene ice sheets in Fig. 4 (right). For the Antarctic study, we choose another contour to characterize the two sub-domes of the Holocene ice sheet (Fig. 8). Obviously, these small circles (or great circles) are too simple for characterizing the migration and accumulation of the ice mass.

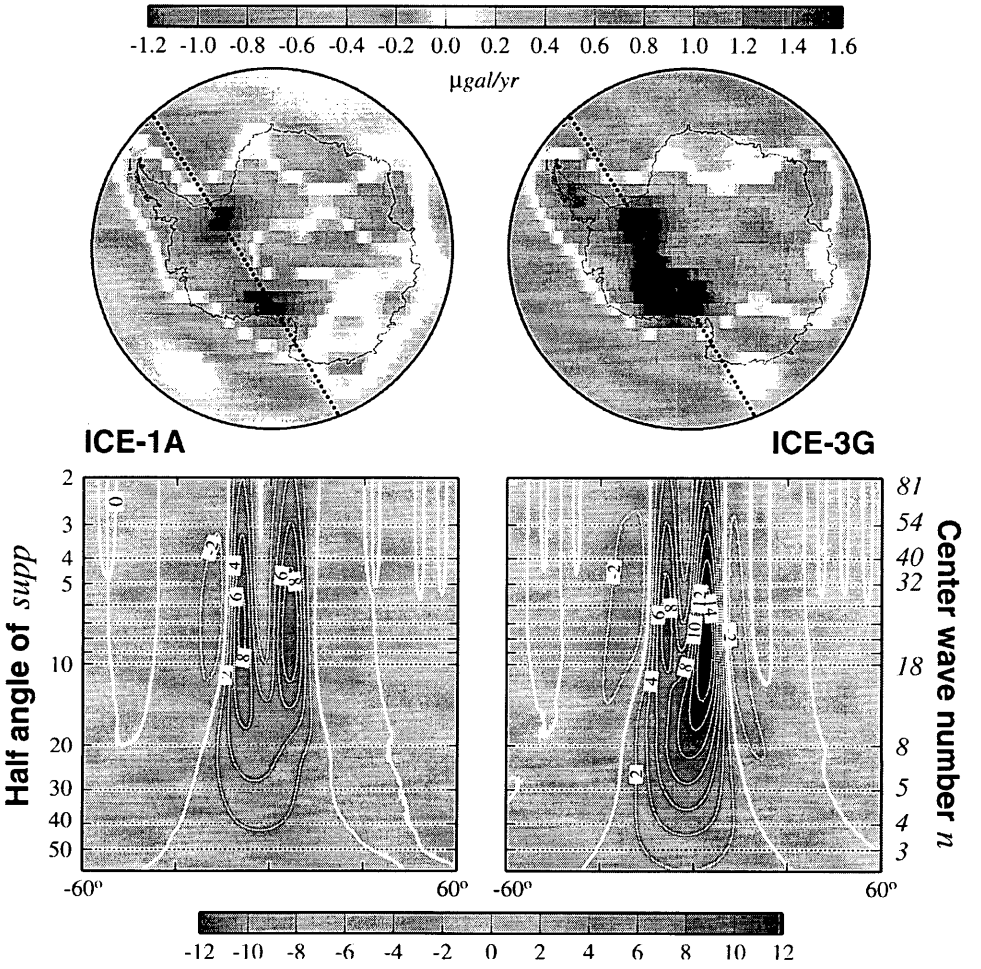


**Fig. 8** Polar projections and wavelet spectrograms for predicted gravity disturbances due to last Quaternary ice sheets in the Antarctic area. The translation operation of the spectrogram is along the diagonal small circle indicated in the polar projections, in order to characterize the two small ice domes. Details of the settings of the spectrogram are referred to the caption of Fig. 4. Predictions are based on a Maxwell Earth with the viscosity model A in Fig. 1 and two ice sheets models. Ice-1A is specified in the figure 3 (see its caption). Ice-3G is from Tushingham & Peltier, 1992). Setting for the polar projections are the same as in Fig. 3.

We are now working on irregular contours for ISW scans. The most promising choices perhaps are the shoreline contours and iso-map contours. Since ice streams, including their surge and discharge, occur along the shorelines (e.g Hughes, 1998). The ISW spectrogram along the shoreline contours should be sensitive to the stream flow and discharge processes. This is important, since most of the uncertainties in the total imbalance come from the discharge processes (see the introduction). We are eager to see the results. But before we can apply the technique to analyze the GRACE data, a large amount of forward modeling has to be done in order to quantify the signature of stream flow and its resolution (the designed resolution for GRACE gravity is about harmonic degree 200, much less for its time variation therefore, resolution is a issue). We have to emphasize again that the ultimate resolution is limited by the raw data. Wavelets cannot create resolution for the raw data, it could only enhance and magnify the existing information blurred with conventional harmonic expansions. We use the digitized mass balance models (e. g. Reeh et al. 1999; Zwally & Giovinetto (2000); Vaughan et al. 1999) as the zero order input to simulate the GRACE gravity observations. We expect to derive the correlation coefficients between the mass change and gravity change in the wavelet transform domain. In order to investigate the sensitivity and resolution, we would manipulate the zero order mass balance model by artificially changing the discharged mass along the shorelines. An important part of this numerical experiment is with the ice shelves in the embayment confined by the shorelines and the calving fronts (the contour along which tabular icebergs are released into the open sea). We also conduct tests to see if the resolution for the volume of the stream flow could be improved by benchmarks with the local ground stations (see the local analysis). These works are time consuming, for the manipulations must be inspected by eye and digitized by hands.

The iso-map contours can be generated either with the digitized topography or mass balance maps. Our ongoing works is similar to what just outlined for the shoreline contours. But here our focus is on quantifying gravity signatures of the accumulation and ablation processes for the ISW along the iso-map contours should be sensitive to accumulation and ablation. Melting is less volatile than surging and calving from ice stream flows, but its distribution is much more complicated. Most of the water bodies are under cover, large amount of meltwater are unable to reach the bed and flow out, because of regelation and refreezing (e.g. Lliboutry, 1998). Melting is more important a mechanism of discharge for Greenland than for Antarctic. Thus, we may regard the shoreline contours as the Antarctic contours, and the iso-map contours as the Greenland contours. While the ISW spectrograms from the two sets of contours are not directly comparable, the end results of inferred mass changes are comparable. Comparison between the two sets of results can serve as a test to see if our strategy really works.

The second target of our on going effort is to quantify a specific mass balance signature identified from ISW transform by inverting it back to recover the original data. In wavelets terminology, it is an issue of data compression and reconstruction. The principle and general procedure of image compression is well known already (e.g. Resnikoff & Wells, 1998). For our purpose, we choose between two opposite quantizers: we either discard the specific mass signature to see its impact on the original data or to strip anything but the specific signatures to see how much the original data could recover. The recovery test is similar to the conventional harmonic analysis (e.g. James & Ivins,

1998; Bentely & Wahr, 1998) except in that the ISW signature in a specific location contributes significantly only to a selected band of harmonic degrees or bandpass filtered, while in a conventional harmonic analysis the mass signature contributes to the full harmonic spectrum. In other words, the ISW mass signature are *characterized* by its harmonic localization (see Fig. 8 for example). An alternative approach is to take some proxy quantities, such as the maximum of the local energy and the related local wave number (Bergeron et al, 1999; 2000). To complete the reconstruction, we have to go through the multresolution analysis (e.g., Freenden & Windheuser, 1996). The discovery of multiresolution analysis (Malat, 1989) perhaps is the ultimate reason for the popularity enjoyed by the wavelet technique today. The basic idea of multiresolution is to split the original signal $f_0$ into a "blurred" component $f_1$ with a coarser resolution and a "detailed" component $d_1$ with a regular resolution. The process repeats itself to split $f_1$ into $f_2$ and $d_2$ ...and go on and on. Similar recursive process can be formulated for the reconstruction. A remarkable thing is that the wavelets representing each $d_n$ form a orthogonal basis with no redundancy. We skip the messy mathematical details except to say that, we have already completed the theoretical perpetration for a multi-resolution analysis based on our particular locally supported ISW, and are ready to write code for the recursive processes. The reason we would like to devote our energy to the multi-resolution analysis is that we could explore the ice mass balance problem from a different prospective, a global view. Our efforts in this part of the investigation are aimed at a multi-resolution inversion for mass balance (accumulation and ablation only) directly from simulated GRACE data. We mention the inversion problem just for a perspective; it is too premature at this stage to set a time frame for its completion.

The price we pay with the ISW analysis is that the spatial localization for the mass balance signature is blurred, again, because of Heisenberg's uncertainty principle. The mathematically exact spatial localization in a conventional harmonic analysis is just an illusion on the physical ground. It is exact only as we put it. But we do not know the exact distribution of subglacial water bodies, the drainage system, and so many other spatial distributions that associated with the mass balances. This is why we believe that wavelet analysis could make a difference in quantifying the total mass imbalances in Greenland and Antarctic areas: we trade the exactness in spatial localization, which we would suffer on the physical ground anyway, for a robust characterization of simultaneous spatial-harmonic localization.

## 4. PROGRESSES OF GLOBAL ANALYSIS

Time variation of lowermost harmonic degrees of the Earth's gravity field, $J_{nm}$, $K_{nm}$ can be regarded as benchmarks for the global mass redistribution (ice +ocean) in complementary to the local benchmarks of individual round measurements. In theory, GRACE is able to achieve better resolution than the satellite laser ranging (SLR). But the scheduled 5 year life time of GRACE already caused concerns that it may be too short for a complete separation between postglacial rebound and the mass migration of the underground hydrology system. A solution to this problem is to work together with SLR to extend its effective life (e.g. Wahr & Han, 1998). The SLR already has more than 25 years of data collection and the effort is continuing. The low degree $J_{nm}$, $K_n$ are sensitive

to mass redistributions not only on the surface, but also in the mantle and even in the core (e.g. Fang et al, 1996). The largest contribution from the interior is postglacial (e.g. Fig. 9). But how sensitive the $J_{nm}$, $K_n$ are to the model ice history is not fully understood, so we conducted, in collaboration with the CSR group at Texas U, the systematic calculations of the $J_{nm}$, $K_n$ in the $\eta_u$~$\eta_l$ plane based on two ice models, ICE-1A and ICE-3G. We can see clearly in Fig. 9 that $J_n$ is capable of distinguishing the two Holocene ice models. This is totally unexpected and encouraging. Recently, our collaborative efforts is directed to identifying the geophysical causes for $J_{nm}$, $K_n$. Our preliminary calculations, from published sources, of surface mass contributions to $J_n$ other than Greenland and Antarctic are listed in the following table. It is evident that Greenland & Antarctica are the major surface contributors.

| *Source* | $J_2$ | $J_3$ | $J_4$ | $J_5$ | $J_6$ | $J_7$ | $J_8$ |
|---|---|---|---|---|---|---|---|
| **Satellite Obs.** | -2.7±0.4 | -1.2±0.5 | -1.1±1.0 | 0.9±1.0 | 0.4±0.5 | -2.4±1.4 | 1.1±0. |
| **Mountain Glacier** | 0.34 | 0.25 | 0.12 | 0.25 | 0.19 | 0.24 | 0.16 |
| **Reservoirs** | -0.08 | -0.01 | 0.11 | 0.19 | 0.20 | 0.14 | < 0.01 |
| **Atmosphere** | 0.17 | 0.04 | 0.18 | 0.08 | 0.08 | 0.01 | 0.01 |
| **Ground water** | 0.2 | | | | | | |
| **Earthquake** | -0.022 | 0.01 | -0.015 | -0.003 | | | |
| **Core rotation** | -0.04 | | <0.001 | | <0.001 | | |

The SLR data processing and surface mass analysis are carried out by the Taxes group. Our job is to constrain the viscosity structure. Viscosity is a multidisciplinary issue, and unlikely to be resolved by the study of the $J_n$. Nonetheless, it is important for us to understand how sensitive the $J_n$ are to the viscosity and how it may affect the estimates of the mass balance. Our preliminary results shown in Fig. 9 are based on a suit of two layer viscosity models. These two layer models are likely oversimplified, considering the real physical conditions in the Earth's interior (e.g. Ranalli, 1998). We have come up with a new parameterization for the "realistic" viscosity models (Fang & Hager, 1999) which relates the models constructed from the microphysics of creeping to a set of parameters tangible with geophysical measurements. Two of such viscosity profiles are shown in Fig. 7. We are conducting similar calculations as shown in Fig. 9 but with a suit of "realistic" viscosity models". We expect to rule out some of the two layer viscosity models, if the predicted $J_n$ deviate significantly from those based on physical consideration and, at the same time, from those observed directly. We do not believe that such a procedure will enable us to sort out between the remaining two-layer viscosity models and the "realistic" viscosity models. Nonetheless, we could use the remaining two-layer mode to set the range of uncertainties for the estimates of the ice mass balance (the realistic viscosity profiles are a little difficult to handle for the purpose of setting error bars).

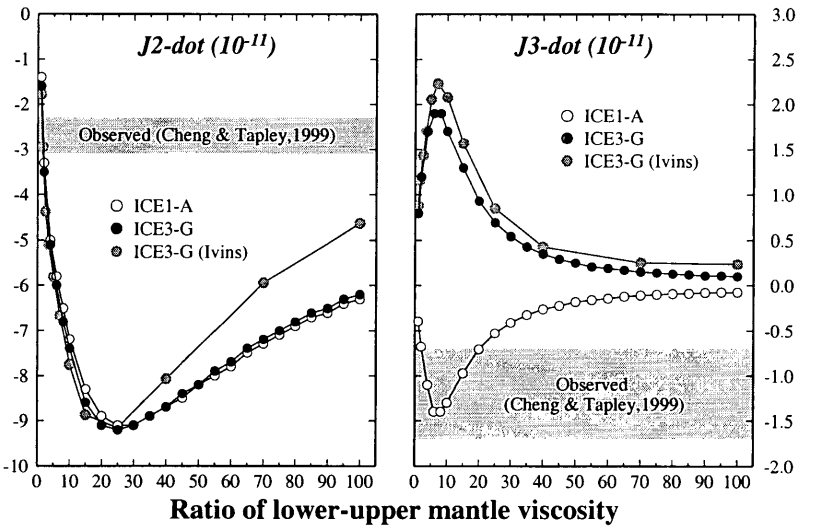


**Fig. 9** Time varying $J_n$ predicted base on postglacial rebound. Two ice models ICE1-A, and ICE3-G are used along with a suite of two-layer viscosity model with the lithosphere fixed at 120 km and the upper mantle viscosity fixed at 10**21 Pas. The predicted are functions of the ratio of lower/upper mantle viscosity. Grey dots are from James & Ivins (1998). Shaded areas indicate the observed with their error bars from SLR (Cheng et al. 1997).

Another issue we are investigating is how deep the $J_n$ can penetrate to sense the change of density associated with viscoelastic relaxation. It is more a geodynamic issue than geodetic. For the mass balance problem it allows us to explore the origin of the error source from the mantle. A method we plan to employ is the analysis of the relaxation time spectrum. As we can see from Fig. 7, the relaxation time spectrum is sensitive to the viscosity structure, and the lower degree relaxation times can penetrate deeper. We are trying to perturb different portions of the viscosity profiles from the elastic lithosphere, upper mantle down to 660km depth, and the lower mantle respectively to examine the responses of the relaxation time spectrum. We expect to provide through this experiment quantitative measures, in percentage, about the contributions from the lithosphere, upper mantle and lower mantles to the total error induced by mantle deformation in the estimates of the mass balances.

Manuscripts for publication are prepared jointly and separately by the two groups. And the results shown in Fig. 9 have already been communicated with the geodynamic groups world wide.

## 5. PROGRES OF SEA LEVEL AND TIDE GAUGE ANALYSIS

### 5.1 Published results

The sea level change associated with glacial isostatic adjustment is one of the classical problems in geophysics. As mentioned earlier, it is a coupled cryosphere-hydrosphere-atmosphere system. The melted ice mass spills into the sea, and rearranges the mass distribution on the surface of the solid Earth. The solid Earth in turn deforms in response

to the redistribution of the surface loads, and causes the sea level to adjust itself to reach an equilibrium with the remaining ice sheets and the deformed solid Earth. The melting of ice sheets has its astronomical causes and strong climatic consequences, while the deformation of the solid Earth depends crucially upon creep processes in the interior. Thus, the dynamics of the coupled system links a broad range of subjects, such as the evolution of planetary orbits, climatology, glaciology, mantle rheology, Earth rotation, and so on.

The notion of a coupled system implies a global treatment, i.e. the volume of ice, sea water, and the solid Earth must be finite. Historically, the study of post glacial sea level started from a local approach (Haskell, 1935, 1937; Vening Meinesz, 1937; Niskannen, 1948) for interpreting elevated beach traces in Fennoscandia. Locally, the ice load has forced the mantle rocks to flow laterally, causing considerable subsidence of the surface beneath the ice. In addition to this dynamic isostasy, the Earth and the ocean in a coupled system have to readjust themselves in responses to the redistribution of the ice load to maintain the toal gravitational potential energy of the system at a minimum. As it turns out, the restoring self-gravitation force against the Earth's readjustment plays an important role in the surface rebound (e.g. Peltier, 1989).

The formulation for global analyses of post glacial sea level was begun by Cathles (1975), and completed by Farrell & Clark (1976) by the establishment of the so called sea level equation. Aside from the melting of ice and the responses of the finite solid Earth, the self-gravitation of the perturbed water load, i.e. the new sea level relative to the deformed sea floor, is also considered in the sea level equation to contribute to the formation of the new sea level itself. This self forcing mechanism makes the sea level equation non-linear. Approximations are implemented for solving the sea level equation at a particular time at a particular site (Farrell & Clark, 1976; Wu & Peltier, 1983; Nakiboglu et al, 1983). This situation is consistent with the fact that the observed sea level variationa are available only at a number of sites along continental shorelines and ocean islands. An effort has been made by Tushingham & Peltier, (1992) to compile the observed relative sea levels from various sources at more than 400 sites. Global solutions are proposed by Mitrovica & Peltier (1991) and Johnston (1993).

A limitation of the site by site analysis is that it is difficult to reveal the physics of the coupled system by looking at individual sites. Often information about the viscosity and ice history is either too complicated to handle or too weak to use at individual sites. An example is the construction of the ICE-3G model (Tushingham & Peltier, 1991, 1992). ICE-3G is constructed by fitting the observed RSL curves with the predicted for a fixed viscosity structure at each individual site. Only 192 sites among nearly 400 were employed because the remaining 200 far field sites are not sensitive to the ice history. Among the 192 used, a large number of the sites located on the margin of former ice sheets are extremely sensitive to the uncertainties in both ice history and the viscosity (Nakada & Lambeck, 1987; Fang & Hager, 1996), hence the effects of viscosity and ice history at these sites are inseparable. It appears that substantial improvement can be made only by simultaneous constraints for both viscosity and ice history. A crucial step toward this goal is to obtain a global coverage of the geoid.

Satellite altimetry, SLR, and especially the GRACE mission provide global coverage for time variations in geoid and sea level. But the satellite data are too recent to help

recreating the RSL history for the past 20,000 years. Isotope dating of the marine deposits along the elevated or subsided shorelines has been the major source for RSL data. Even in an ideal situation where the isotope data are collected continuously along the beaches all over the world, the data coverage is only one dimensional. Can we recover a 2-D distribution out of a set of 1-D data? An issue relating to the answer is the smoothness of the 2-D field. The importance of smoothness to the recovery of the 2-D RSL is demonstrated by the following two extremes A perfectly smooth sea surface is the eustatic sea level. In this case the 2-D RSL can be recovered by the knowledge at only one site. A perfect non-smooth sea level is an extremely localized random type of distribution where the characteristic length for causal correlation between two points is nearly zero. The recovery of a total 2-D field from any kind of partial knowledge, 1-D, or 2-D is impossible.

In this work we further explore the physics of the cryosphere-hydrosphere-atmosphere system. We first derived the sea level equation based on least potential energy principle. A global solution is also derived following the same spirit. Using the global solution, we next examine the smoothness of the global RSL. Our method is forward modeling on a laterally homogeneous Maxwell viscoelastic Earth using a number of admissible "realistic" viscosity models. We demonstrated that the horizontal smoothness of the RSL also relates to the sensitivity of RSL to the intra lithospheric structure. Parameterization of realistic viscosity models in itself an important issue. We propose a phenomenological parameterization. Based on microphysical considerations and seismic observations. This new parameterization can be directly constrained with geological observations. A lithosphere by definition suppresses viscous relaxation. We examine the effects of the lithosphere thickness on the sensitivity of RSL to "realistic" viscosity structures by comparing the predicted RSL for different lithosphere models. At a number of individual sites. We find that satisfactory convergence of global sea level solution can be reached at about harmonic degree 50. And the convergence appears independent of the ice model. This relatively lower tolerable truncation level is a consequence of global nature of the ice-sea-earth system. Variation of lithosphere thickness does not alter our previous conclusions (Fang & Hager, 1996) that there is a correlation of the RSL sensitivities between ice history and viscosity structures: at sites less sensitive to the ice model, the resolving power for viscosity structure is also less. Furthermore, models having a thicker lithosphere tend to permit better resolution of lower mantle viscosity.

**5.2 Results to be published**

The total ice mass imbalance from the continent is complementary to the total water imbalance in the ocean. The surface of an isothermal ocean at equilibrium can be derived based on the least potential energy principle (Fang & Hager, 1999). This steady state ocean is implicitly assumed in most of the geodetic sea level problems. The flowing ocean should also satisfy some least energy principle. The difficulty is how to specify those energies, especially the energies associated with the thermal transport processes. Dynamic effects superimposed on the steady ocean and local tectonics perhaps are the major error sources for the estimates of sea level variation from tidal gauge analysis.

We conducted a comparative study on the tidal gauge records from different regions. Our focus is on the Far-East coastal areas where the post glacial rebound effects are fairly small (see Fang & Hager, 1999 for specific sites in the Tokyo Bay area). A large number of tidal gauge records have been collected by the geodetic group in the Hong Kong Polytech. University over the last two decade (Ding et al., 2001). Fig. 10 shows the sea level variation derived from tide gauge records from the 1950's to present at the Shanghai and Hong Kong stations. They both exhibit increases at about 2mm/yr. level, but the discrepancy, 0.6 mm/yr. is too conspicuous to ignore. This part of the investigation is in collaboration with the geodetic group at the Hong Kong Polytech. U. They have independent resources for their research projects under the International Program of "Asia Pacific Space Geodynamics".

The Hong Kong group has worked on the selection processes for the reliable sites and processing the data. Our expectation is to see if there are regularities from the discrepancies through the suit of sites. We are running our sea level code developed during this project to provide an improved steady state sea level. The present day steady state sea level have been calculated repeatedly (e.g. Conrad & Hager, 1997; Mitrovica et al, 2001) based on the equal potential theory of Farrell & Clark (1976) and simplified models of ice mass imbalances. We will use our least potential energy formulation (Fang & Hager, 1999) and new models of mass imbalance estimated based on cross constraints form local, regional, and global analysis. For a decadal time scale, an elastic reference Earth is adequate, thus, the computations are much simpler than for postglacial sea levels

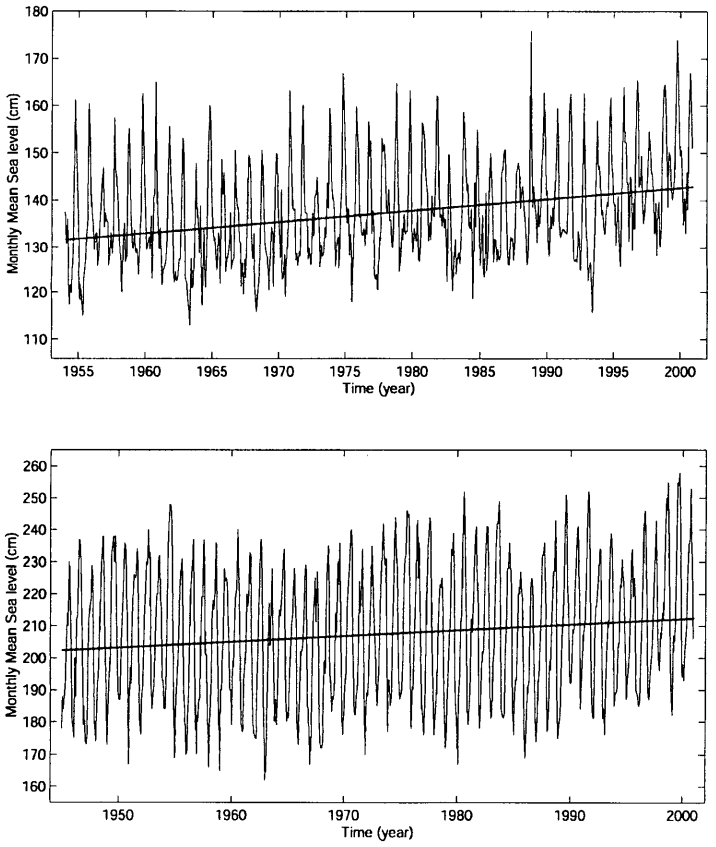


**Fig. 10** Upper panel, the monthly mean sea level change in Shanghai sea area during the time span of 1945.0 ~ 2001.0 recorded from Wusong tide gauge station. The tide gauge data has been adjusted for land settlement by levelling measurements. The blue line shows a rising tendency with a rate of 1.79±0.19 mm/yr . Lower panel, Same as upper except that it is of Hong Kong sea area during the time span of 1954.0 ~ 2001.0 recorded from North Point and Quarry Bay. The blue line shows a rising tendency with a rate of 2.39±0.20 mm/yr. Source form Ding et al (2001) and Dawei Zheng of Hong Kong Polytech. U.

where an Maxwell viscoelastic Earth must be employed. We are waiting for the number to conduct a preliminary assessment of how reliable these tidal gauge results are in terms of relating them to the eustatic sea level change and mass imbalances. Results of this collaborative work will be published soon both jointly and separately by our two groups.

## 6. LIST OF PUBLICATIONS

### 6.1 Peer reviewed papers

Fang, M. and B. H. Hager, 1999. Postglacial sea level: energy method, *Global & Planet. Change*, **20**, 125-156.

Fang, M. & B. H. Hager, 2001. Vertical deformation and absolute gravity, *Geophys. J. Int.*, **146**, 539-548.

Fang., M. and B. H. Hager, 2002. On the apparent exponential relaxation curves at the central regions of the last Pleistocene ice sheets, *J. Geophys. Res.* (special issue) in press.

Fang, M. and B. H. Hager, 2002, Postglacial rebound signatures in GRACE by a spherical wavelet filer, *in preparation.*

Fang, M. W. Kuang, B. Chao, & B. H. Hager, 2002, Mantle tidal shielding of the gravity perturbations from the core, *in preparation.*

Cheng, M., M. Fang, B. H. Hager, and B. D. Tapley, 2002. Constraining the distribution of ice sheets by secular variations in the Earth's gravity field , *in preparation.*

### 6.2 Conference presentations

Fang, M. B. H. Hager, 1998. Spherical wavelets and the relaxation spectrum of post glacial rebound, , *EOS, Trans. AGU* Vol. **79**, **45**, F886.

Cheng, M., M. Fang, and B. D. Tapley, 1999. Secular variations in the Earths gravity field and ice sheet mass balance, , *EOS, Trans. AGU* Vol. **80**, **46**, F249.

Aharoson, O., B. H. Hager,, M. Fang, and S. Zhong, 1999. Mars: viscoelastic responses and planetary rotational dynamics, , *EOS, Trans. AGU* Vol. **80**, **46**, F628.

Hager, B. H. and M. Fang, 1999. Dislocation-induced static deformation of a self-gravitating multi layer elastic half space, , *EOS, Trans. AGU* Vol. **80**, **46**, F935.

Fang, M. W. Kuang, B. Chao, & B. H. Hager, 1999, Mantle tidal shielding, *EOS, Trans. AGU* Vol. **80**, **46**, F23.

Fang, M. and B. H. Hager, 2000. Post glacial rebound calibration for GRACE by combining with GPS verticals, , *EOS, Trans. AGU* Vol. **81**, **48**, F311.

Cheng, M., M. Fang, B. H. Hager, and B. D. Tapley, 2000. Constraining the distribution of ice sheets by secular variations in the Earth's gravity field, , *EOS, Trans. AGU* Vol. **81**, **48**, F319.

Fang, M. B. H. Hager, 2001. Major Holocene ice sheet signatures in the GRACE data, , *EOS, Trans. AGU* Vol. **82**, **47**, F291.

## 7. REFERENCES


Bamber, J. L., 1994. A digital elevation model of the Antarctic ice sheet derived from the ERS-1 altimeter data and comparison with terrestrial measurements, *Ann. Glaciol.*, **20**, 48-54.

Bamber, J. L and P. Huybrechts, 1996. Geometric boundary conditions for modeling the velocity field of the Antarctic ice sheet, *Ann. Glaciol.* **23**, 364-373.

Bard, E., B. Hamelin, R. G. Fairbank, and A. Zindler, 1990. Calibration of the 14C timescales over the past 30,000 years using mass spectrometric U-Th ages from Barbados corals, *Nature*, **345**, 405-410.

Bentley, C. R. and J. M. Wahr, 1998. Satellite gravity and the mass balance of the Antarctic ice sheet, *J. Glaciol.* **44**, 207-213.

Bergeron, S. Y., A. P. Vicent, D. A. Yuen, Tranchant, J. S., and C. Tchong, 1999. Viewing seismic velocity anomalies with 3-D continuous Gaussian wavelets, *Geophys. Res. Lett.*, **26**, 15, 2311-2314.

Bergeron, S. Y., D. A. Yuen, and A. PP. Vicent, Capability of 3-D wavelet transforms to detect plume-like structures from seismic tomography, *Geophys. Res. Lett.*, **27**, 20, 3433-3436.

Bethoux, N., G. Ouillon, and M. Nicolas, 1998. The instrumental seismicity of the Western Alps: spatial-temproal patterns analyzed with the wavelet transform, *Geophys. J Int.*, **138**, 177-194.

Bull, C., 1971. *Snow Accumulation in Antarctica: Research in the Antarctic*, American Associ. Adv. Sci.

Cathles, L. M., 1975. *The viscosity of the Earth's Mantle*, Princeton Univ. Press.

Cheng, M. C. K. Shum, and B. D., Tapley, 1997. Determination of long term changes in the Earth's gravity field from satellite laser ranging observations, *J. Geophys. Res.* **102**, 22,377-22,390.

Conrad, C. P. and B. H. Hager, 1997. Spatial variations in the rate of sea level rise caused by the present day melting of glaciers and ice sheets, *Geophys. Res. Lett.*, **24**, 1503-1506.

Dahlen, F. A., 1976. The passive influence of the oceans upon the rotation of the earth, *Geophys. J. R. astron. Soc.*, **46,** 363-406.

Denton, G. H., T. Hughes, and W. Karlen, 1986. Global ice-sheet system interlocked by sea level, *Quart. Res.*, **26**, 3-26.

Ding Xiaoli, Zheng Dawei, Chao Jason, Chen Yongqi, Li Zhilin Li, 2001. *Sea level change in Hong Kong from tide gauge measurements of 1954 - 1999. Journal of Geodesy*, **74** 683-689.

Douglas, B. C., 1991. Global sea level rise, *J. Geophy. Res.*, **96**, 6981-6992.

Douglas, B. C., 1997. Global sea level rise: a redetermination, *Surv. Geophys.* **18**, 279-292

Dziewonski, A. M. and D. L Anderson, 1981. Preliminary reference Earth model, *Phys. Earth Planet. Inter.*, **25,** 297-356.

Ekman, M., 1992. Postglacial rebound and sea level phenomena, with special reference to Fennoscandia and the Baltic sea, Lecture note, *NKG Autumn School Helsinki, Nordic Geodetic Commission*, XX, 229-234.

Ekman, M. and J. Makinen, 1996. Recent post glacial rebound, gravity change and mantle flow in Fennoscandia, *Geophys. J. Int.*, 126, 229-234.

Fang, M. and B. H. Hager, 1995. The singularity mystery associated with a radially continuous Maxwell viscoelastic structure, *Geophys. J. Int.*, **123**, 849-865.

Fang, M. and B. H. Hager, 1996. The sensitivity of post-glacial sea level to viscosity structure and ice-load history fro realistically parameterized viscosity profiles, *Geophys. Res. Lett.*, **23**, 3787-3790.

Fang, M., B. H. Hager and T. A. Herring, 1996. Surface deformation caused by pressure changes in the fluid core, *Geophys. Res. Lett.*, **23**, 1493-1496.

Fang, M. and B. H. Hager, 1999. Postglacial sea level: energy method, *Global & Planet. Change*, **20**, 125-156.

Fang, M. & B. H. Hager, 2001a. Vertical deformation and absolute gravity, *Geophys. J. Int.*, **146**, 539-548.

Fang., M. and B. H. Hager, 2001b. On the apparent exponential relaxation curves at the central regions of the last Pleistocene ice sheets, *J. Geophys. Res.* (special issue) in press.

Fang, M., M. Simons, and B. H. Hager, 1995. The Hudson Bay gravity anomaly and postglacial rebound, (Abstract) *EOS, Trans. American Geophys. Union*, **76,** No. 46, 158.

Farrell, W. E. and J. A. Clark, 1976. On postglacial sea level, *Geophys. J. R. astr. Soc.*, **46**, 647-667.

Freenen W. and U. Windhuser, 1996. Spherical wavelet transform and its discretization, *Adv. comput. Math.*, **5**, 51-94.

Freenen W. and U. Windhuser, 1997. Combined spherical harmonic and wavelet expansion- a future concept in Earth's gravitational determination, *Appl. Comput. Harmonic Anal.*, **4**, 1-37.

Giovinetto, M. B. and C. R. Bentley, 1987. Surface balance in ice drainage systems of *Antarctica, Ant. J. U. S.*, **20**, 6-13.

Hager, B. H., 1989. Mantle viscosity: a comparison of models from postglacial rebound and from the geoid, plate driving force, and advected heat flux, in *Glacial Isostasy Sea-Level and Mantle Rheology*, ed. R. Sabadini, K. Lambeck, and E. Boschi, Nato ASI Ser. C334, Kluwer Acad. Publi., 493-513.

Hager, B. H., 1991. Weighing the ice sheets using space geodesy: a way to measure changes in ice sheet mass, *EOS, Trans. AGU*, **17**, 91.

Haskell, N. A., 1935. Th motion of a fluid under a surface load,1, *Physics*, **6**, 265-269.

Hughes, T., 1987. Ice dynamics and deglaciation models when ice sheets collapsed, in Rudiman W. F. & H. E. Wright (eds) *North America and Ajacent Oceans During the Last Deglaciation*, pp 183-220, Geological Society of America, Boulder.

Hughes, T. *Ice Sheets*, 1998. Oxford U. Press.

Jacobs, S. S. H. H. Helmer, C. S. M. Doakes, A. Jenkins, and R. M. Frolich, 1992. Melting of ice shelves and the mass balance of Antarctica, *J. Glaciol.*, **38**, 375-387.

James, T. S., 1992. The Hudson Bay free-air gravity anomaly and glacial rebound, *Geophys. Res. Lett.*, **19**, 861-864.

James T. H. and E. R. Ivins, 1998. Predictions of Antarctic crustal motions driven by present dayice sheet evolution and by isostatic memory of the last glacial maximum, *J Geophys. Res.*, **103**, 4993-5017.

Johnston, P., 1993. The effect of spatially non-uniform water loads on prediction of sea level change, *Geophys. J. Int.*, **114,** 615-634.

Lambeck, K., P. Johnston, and M. Nakada, 1990. Holocene glacial rebound and sea-level change in NE Europe, *Geophys. J. Int.*, **103**, 451-468.

Larson, K. M. and T. van Dam, 2000. Measuring postglacial rebound with GPS and absolute gravity, *Geophys. Res. Lett.*, **27**, 3925-3928.

Liboutry, L., 1998. How to model the waxing and waning of ice sheets, in *Glacial Isostasy Sea-Level and Mantle Rheology*, ed. R. Sabadini, K. Lambeck, and E. Boschi, Nato ASI Ser. C334, Kluwer Acad. Publi., 249-270.

McConnell, R. K., 1968, Viscosity of the mantle from relaxation time spectra of isostatic adjustment, *J. Geophys. Res.*, **73**, 7089-7105.

Mitrovica, J. X, 1996. Haskell [1935] revisited, *J. Goephys. Res.*, **101**, 555-569.

Mitrovica, J. X., and W. R. Peltier, 1991. On postglacial geoid subsidence over the equatorial oceans, *J. Geophys. Res.*, **96**, 20,053-20,071.

Mitrovica, J. X. and R. W. Peltier, 1993. A new formalism for inferring mantle viscosity based on estimates of post-glacial decay time: application to RSL variations in N.E. Hudson Bay, *Geophys. Res. Lett.*, **20**, 2183-2186.

Mitrovica, J. X. and W. R. Peltier, 1995. Constraints on mantle viscosity based upon the inversion of post-glacial uplift data from the Hudson Bay region, *Geophys. J. Int.* **122**, 353-377.

Mitrovica J. X., A. M. Forte, and M. Simons, 2000. A reappraisal of post glacial decay times from Richmond Gulf and James Bay, Canada, *Geophys. J. Int.*, **142**, 783-800.

Mitrovica J. X. M. E. Tamisiea, J. L. Davis, and G. Milne, 2001. Recent mass balance of polar ice sheets inferred from patterns of global sea level change, *Nature*, **409**, 1026-1029.

Nakada, M and K. Lambeck, 1987. Glacial rebound and relative sea-level variation: a new appraisal, *Geophys. J. R. Astr. Soc.*, **90**., 171-224.

Nerem, R. S., et al, Gravity model development for TOPEX/POSEIDON: joint gravity models 1 and 2, *J. Geophys. Res.*, **99**, 24,421-24,447.

Peltier, W. R., 1996. Ice age Palaeotopography, *Science*, **265**, 195-201.

Peltier, W. R. and J. T. Andrews, 1976. Glacial isostatic adjustment I, the forward problem, *Geophys. J. R. astro. Soc.*, **46**, 605-646.

Peltier, W. R., A. M. Forte, J. X. Mitrovica, and A. M. Dziewonski, 1992, Earth's gravitational field: seismic tomography resolves the enigma of the Laurentian anomaly, *Geophys. Res. Lett.*, **19**, 1555-1558.

Ranalli, G., 1998. Inference on mantle rheology from creep laws, in *Dynamics of the Ice Age Earth*, ed. P. Wu, Trans. Tech. Publi. Swizerland, 323-340.

Reeh, N., C. Mayer, H. Miller, H. H. Thomsen, and A. Weidick, 1999. Present and past climate control on Fjord glaciations in Greenland: implications for IRD-deposition in the sea, *Geophys. Res. Lett.*, **26**, 1039-1042.

Resnikoff, H. L. and R. O. Wells, 1998. *Wavelet Analysis: the Scalable structure of information*, Springer-Verlag.

Rignot, E., R. Forster, and B. Isacks, 1996. Radar Interferometric observations Glacier San Rafael, Chile, *J. Glaciol.*, **42**, 279, 291.

Rignot, E., 1997. North and Northeast Greenland ice discharge from satellite radar interferometry, *Science*, **276**, 934-937.

Rignot, E.,1998. Fast recession of a west Antarctic glacier, *Science*, **281**, 549-551.

Simons, M., 1995. Localization of gravity and topography: constraints on the tectonics and mantle dynamics of Earth and Venus, *Ph.D. Thesis*, MIT.

Simons, M. and B. H. Hager, 1997. Localization of the gravity field and the signature of glacial rebound, *Nature*, **390**, 500-504.

Tushingham, A. M. and W. R. Pelter, 1991. ICE-3G: a new global model of Wurm-Wisconsin deglaciation using a global data base of relative sea level history, *J. Geophys. Res.* **97**, 3285-3304.

Tushingham, A. M. and W. R. Pelter, 1992. Validation of the ICE-3G model of Wurm-Wisconsin deglaciation using a global data base of relative sea level histories, *J. Geophys. Res.*, **97**, 3285-3304.

Wahr J., 1996. Secular variation of the geoid, with implications for future satellite gravity missions, Trans. Am. Geophys. Union (EOS), 77, f133.

Wahr, J.., D. Han, and A. Trupin, 1995. Predictions of vertical uplift caused by cahnging polar ice volumes on a visco-elastic Earth.

Walcott, R. E., 1980. Rheology models and observational data of glacio-isostatic rebound, in *Earth Rheology, Isostasy and Eustasy,* ed. N. Möner, 3-10. John Wiley & Sons, New York.

Wieczerkowski, K, J. X. Mitrovica, and D. Wolf, 1999. A revised relaxation-time spectrum for Fennoscandia, *Geophys. J. I.*, **139**, 69-86.

Woodworth, P. L., D. T. Pugh, J. G. De Ronde, R. A. Warrick, and J. Hannah, 1992. (eds) *Sea Level Changes: Determination and Effects*, AGU, Washington.

Wu, P. and W. R. Peltier, 1982. Viscous gravitational relaxation, *Geophys. J. R. Astr. Soc.*, **70**, 435-485.

Wu, P. and W. R. Peltier, 1983. Glacial isostatic adjustment and the free air gravity anomaly as a constraint on deep mantle viscosity, *Geophys. J. R. Soc.*, **74**, 377-449. ,

Vaughan, D. J. L. Bamber, M. Giovinetto, J. Russell, and A. P. R. Cooper, 1999. Reassessment of net surface mass balance in Antarctica, *J. Climate*, *April*, 933-941.

Zwally H. J., and M. Giovinetto, 2000. Spatial distribution of surface mass balance on Antarctic, *Ann. Glaciol.*, 31.